Inorganic Chemistry
Article

Inorg. Chem. **2011**, *50*, 1105–1115 **1105**
DOI: 10.1021/ic1019422

Spectroscopic and Structural Investigations Reveal the Signaling Mechanism of a Luminescent Molybdate Sensor

Vincent A. Corden, Anne-K. Duhme-Klair,* Sarah Hostachy, Robin N. Perutz, and Nicole Reddig

Department of Chemistry, University of York, York YO10 5DD, U.K.

Hans-Christian Becker[†] and Leif Hammarström

Department of Photochemistry and Molecular Science, Uppsala University, P.O. Box 523, S-75120 Uppsala, Sweden. [†] Present address: Physical Chemistry, Department of Chemical and Biological Engineering, Chalmers University of Technology, SE-41296 Gothenburg, Sweden

Received September 22, 2010

A heteroditopic ligand **H_2-L** consisting of a dihydroxybenzene (catechol)-unit linked via an amide bond to a pyridyl-unit and its methyl-protected precursor **Me_2-L** were synthesized, characterized, and their photophysical properties investigated. The three accessible protonation states of the ligand, **H_3-L**$^+$, **H_2-L**, and **H-L**$^-$, showed distinct ^{1}H NMR, absorption and emission spectroscopic characteristics that allow pH-sensing. The spectroscopic signatures obtained act as a guide to understand the signaling mechanism of the luminescent pH and molybdate sensor [Re(bpy)(CO)$_3$(**H_2-L**)]$^+$. It was found that upon deprotonation of the 2-hydroxy group of **H_2-L**, a ligand-based absorption band emerges that overlaps with the Re(dπ)→bpy metal-to-ligand charge transfer (MLCT) band of the sensor, reducing the quantum yield for emission on excitation in the 370 nm region. In addition, deprotonation of the catechol-unit leads to quenching of the emission from the Re(dπ)→bpy ^{3}MLCT state, consistent with photoinduced electron transfer from the electron-rich, deprotonated catecholate to the Re-based luminophore. Finally, reaction of 2 equiv of [Re(bpy)(CO)$_3$(**H_2-L**)]$^+$ with molybdate was shown to give the zwitterionic Mo(VI) complex [MoO$_2${Re(CO)$_3$(bpy)(**L**)}$_2$], as confirmed by electrospray ionization (ESI) mass spectrometry and X-ray crystallography. The crystal structure determination revealed that two fully deprotonated sensor molecules are bound via their oxygen-donors to a *cis*-dioxo-MoO$_2$ center.

Introduction

Metal-based luminophores with appended dihydroxybenzene (catechol)-units are known to function as sensors,[1−3] redox switches,[4] photo-[5,6] and electrocatalysts.[7] Functionalized [Ru(bpy)$_3$]$^{2+}$-type luminophores are still the most commonly studied in the field, but [Re(bpy)(CO)$_3$L]-type luminophores (with bpy = 2, 2′-bipyridine and L = monodentate axial ligand, such as a halide or pyridine-derivative) are now proving almost as versatile.[8−14]

Several catechol- or phenol-linked pyridine derivatives that are structurally related to the pyridine-derivative used as the axial ligand in our study have recently been developed, and their pH-dependent photophysical properties have been studied.[15−17] A phenol-pyridinium biaryl chromophore, for

*To whom correspondence should be addressed. E-mail: akd1@york.ac.uk.

(1) Beer, P. D. *Chem. Commun.* **1996**, 689.
(2) Costa, I.; Fabbrizzi, L.; Pallavicini, P.; Poggi, A.; Zani, A. *Inorg. Chim. Acta* **1998**, *275−276*, 117.
(3) O'Bian, L.; Duati, M.; Rau, S.; Guckian, A. L.; Keyes, T. E.; O'Boyle, N. M.; Serr, A.; Görls, H.; Vos, J. G. *J. Chem. Soc., Dalton Trans.* **2004**, 514.
(4) Goulle, V.; Harriman, A.; Lehn, J.-M. *J. Chem. Soc., Chem. Commun.* **1993**, 1034.
(5) Whittle, B.; Everest, N. S.; Howard, C.; Ward, M. D. *Inorg. Chem.* **1995**, *34*, 2025.
(6) Shukla, A. D.; Whittle, B.; Bajaj, H. C.; Das, A.; Ward, M. D. *Inorg. Chim. Acta* **1999**, *285*, 89.
(7) Storrier, G. D.; Takada, K.; Abruna, H. D. *Inorg. Chem.* **1999**, *38*, 559.
(8) Lewis, J. D.; Perutz, R. N.; Moore, J. N. *J. Phys. Chem.* **2004**, *108*, 9037.
(9) Lewis, J. D.; Perutz, R. N.; Moore, J. N. *Chem. Commun.* **2000**, 1865.
(10) Schanze, K. S.; MacQueen, D. B.; Perkins, T. A.; Cabana, L. A. *Coord. Chem. Rev.* **1993**, *122*, 63.
(11) Sun, S.-S.; Lees, A. J. *Coord. Chem. Rev.* **2002**, *230*, 171.
(12) Kirgan, R. A.; Sullivan, B. P.; Rillema, P. *Top. Curr. Chem.* **2007**, *281*, 45.
(13) Kumar, A.; Sun, S.-S.; Lees, A. J. *Top. Organomet. Chem.* **2010**, *29*, 1.
(14) Lo, K. K.-W.; Louie, M.-W.; Zhang, K. Y. *Coord. Chem. Rev.* **2010**, *254*, 2603.
(15) Basaric, N.; Wan, P. *Photochem. Photobiol. Sci.* **2006**, *5*, 656.
(16) Kaneko, S.; Yotoriyama, S.; Koda, H.; Tobita, S. *J. Phys. Chem.* **2009**, *113*, 3021.
(17) Jacoby, C.; Böhm, M.; Vu, C.; Ratzer, C.; Schmitt, M. *ChemPhysChem* **2006**, *7*, 448.

Published on Web 01/10/2011

Scheme 1. Structures of the Accessible Protonation States of $[Re(bpy)(CO)_3(\mathbf{H_2\text{-}L})]^+$, $[Re(bpy)(CO)_3(\mathbf{Bn_2\text{-}L})]^+$, $\mathbf{H_2\text{-}L}$, and $\mathbf{Me_2\text{-}L}$, with Most Likely Intramolecular Hydrogen-Bond Arrangements Indicated in Each Case

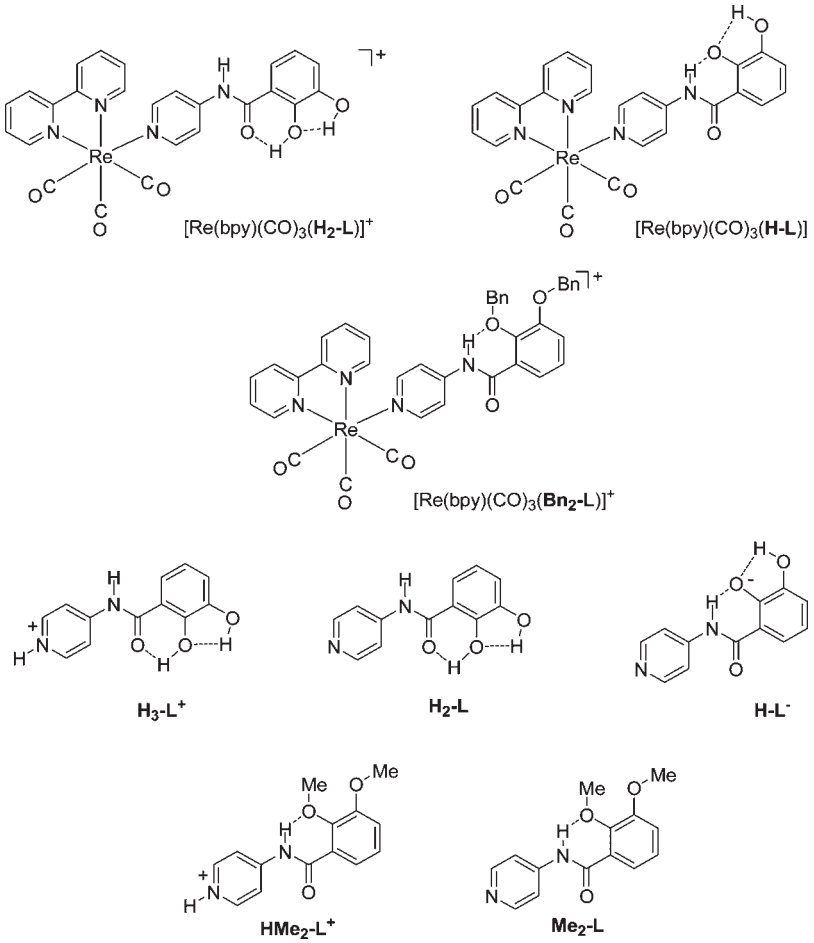

example, has been investigated as potential photoacid.[18] In addition, pyridine-linked catechol[19] or phenol[20] derivatives with more than one protonation state have shown promise as wide-range or ratiometric pH sensors.

We are interested in catechol-appended luminophores since they can be applied in the sensing of biologically relevant oxometalates, such as molybdate, tungstate, or vanadate.[21] In our previous work, we have developed a series of luminescent chemosensors for such species,[22−24] with potential analytical applications in environmental monitoring,[25] biochemical research,[26,27] and medical analysis.[28,29] For these applications, selectivity for oxometalates over oxoanions, such as SO_4^{2-} and HPO_4^{2-}, which resemble MoO_4^{2-} and HVO_4^{2-} in size, shape, and charge, is a key requirement. High selectivity can be achieved with catecholate-based binding units since the transition metal centers are able to coordinate to catecholates by enhancing their coordination number to six,[30−32] while sulfur and phosphorus cannot react in this way. In addition, selectivity for oxometalates over cations, such as Fe(III) or Cu(II) can be achieved by pH-control.[22]

The molybdate sensor $[Re(bpy)(CO)_3(\mathbf{H_2\text{-}L})]^+$ (Scheme 1), in which the catechol-unit is connected to the monodentate pyridyl ligand of the luminophore via an amide linker, signals the presence and concentration of molybdate (MoO_4^{2-}) in solution through a decrease in luminescence intensity.[23] Here we report the results of a combined spectroscopic and structural study to further characterize the signaling mechanism that gives rise to the decrease in the emission intensity of the sensor upon deprotonation or analyte binding.

(18) Malval, J.-P.; Diemer, V.; Morlet Savary, F.; Jacques, P.; Allonas, X.; Chaumeil, H.; Defoin, A.; Carre, C. *Chem. Phys. Lett.* **2008**, *455*, 238.
(19) Evangelio, E.; Hernando, J.; Imaz, I.; Bardaji, G. G.; Alibes, R.; Busque, F.; Ruiz-Molina, D. *Chem.—Eur. J.* **2008**, 9754.
(20) Charier, S.; Ruel, O.; Baudin, J.-B.; Alcor, D.; Allemand, J.-F.; Meglio, A.; Jullien, L.; Valeur, B. *Chem.—Eur. J.* **2006**, *12*, 1097.
(21) Duhme-Klair, A.-K. *Eur. J. Inorg. Chem.* **2009**, 3689.
(22) Jedner, S. B.; James, R. J.; Perutz, R. N.; Duhme-Klair, A.-K. *J. Chem. Soc., Dalton Trans.* **2001**, 2327.
(23) Peacock, A. F. A.; Batey, H. D.; Rändler, C.; Whitwood, A. C.; Perutz, R. N.; Duhme-Klair, A.-K. *Angew. Chem., Int. Ed.* **2005**, *44*, 1712.
(24) Batey, H. D.; Whitwood, A. C.; Duhme-Klair, A.-K. *Inorg. Chem.* **2007**, *46*, 6516.
(25) Mason, J. *Toxicology* **1986**, *42*, 99.
(26) Pau, R. N.; Lawson, D. M. In *Metal Ions in Biological Systems*; Sigel, H., Sigel, A., Eds.; Marcel Dekker: New York, 2002; p 32.
(27) Kuper, J.; Llamas, A.; Hecht, H.-J.; Mendel, R. R.; Schwarz, G. *Nature* **2004**, *430*, 803.
(28) Shih, V. E.; Abroms, I. F.; Johnson, J. L.; Carney, M.; Mandell, R.; Robb, R. M.; Cloherty, J. P.; Rajagopalan, K. V. *N. Engl. J. Med.* **1977**, *297*, 1022.
(29) Kisker, C.; Schindelin, H.; Pacheco, A.; Wehbi, W. A.; Garrett, R. M.; Rajagopalan, K. V.; Enemark, J. H.; Rees, D. C. *Cell* **1997**, *91*, 973.
(30) Kustin, K.; Liu, S.-T. *J. Am. Chem. Soc.* **1973**, *95*, 2487.
(31) Duhme-Klair, A.-K.; Vollmer, G.; Mars, C.; Fröhlich, R. *Angew. Chem., Int. Ed.* **2000**, *39*, 1626.
(32) Liu, C.-M.; Nordlander, E.; Schmeh, D.; Shoemaker, R.; Pierpont, C. G. *Inorg. Chem.* **2004**, *43*, 2114.

The Re(I)-center in $[Re(bpy)(CO)_3(\mathbf{H_2\text{-}L})]^+$ is coordinated to two electron-poor acceptor ligands, the bpy ligand and the pyridine-unit of $\mathbf{H_2}$**-L**. In contrast, the 2, 3-dihydroxybenzamide-unit of $\mathbf{H_2}$**-L** is electron rich and becomes reducing upon deprotonation. Upon UV/vis excitation, several charge transfer transitions are thus conceivable for the deprotonated form of sensor $[Re(bpy)(CO)_3(\mathbf{H\text{-}L})]$, including Re(d$\pi$)→bpy metal-to-ligand charge transfer (MLCT), intraligand charge transfer from the deprotonated catecholate to the pyridine-unit (ILCT), and ligand-to-ligand charge transfer (LLCT) from the deprotonated catecholate unit to the bpy ligand.

To facilitate the interpretation of the electronic absorption and emission spectra of $[Re(bpy)(CO)_3(\mathbf{H\text{-}L})]$, we have synthesized the benzyl-protected derivative $[Re(bpy)(CO)_3(\mathbf{Bn_2\text{-}L})]^+$, the ligand $\mathbf{H_2}$**-L**, and its methyl-protected derivative $\mathbf{Me_2}$**-L** to serve as control compounds. The benzyl-protected sensor cannot deprotonate and shows the spectroscopic characteristics of Re(dπ)→bpy charge transfer (MCLT). In addition, pH-dependent studies of the ligand $\mathbf{H_2}$**-L** provide the spectroscopic signatures of its three accessible protonation states, $\mathbf{H_3}$**-L**$^+$, $\mathbf{H_2}$**-L**, and **H-L**$^-$. The comparison of the spectroscopic characteristics of $[Re(bpy)(CO)_3(\mathbf{Bn_2\text{-}L})]^+$, $\mathbf{H_3}$**-L**$^+$, $\mathbf{H_2}$**-L**, **H-L**$^-$, $\mathbf{HMe_2}$**-L**$^+$, and $\mathbf{Me_2}$**-L** with those of the molybdate sensor in its protonated and deprotonated states, $[Re(bpy)(CO)_3(\mathbf{H_2\text{-}L})]^+$ and $[Re(bpy)(CO)_3(\mathbf{H\text{-}L})]$, respectively, allows identification of important aspects of the photophysical processes involved in the signaling mechanism.

The time-resolved infrared spectra of $[Re(bpy)(CO)_3L]$ complexes show strong carbonyl bands, the position of which reflects the electron density of the Re-center. MLCT excited states give rise to high frequency shifts of the carbonyl bands, whereas photoinduced electron transfer from ligands appended to the Re-center causes low frequency shifts.[33−37] A related paper will be published in due course, describing insights obtained by time-resolved IR spectroscopy. These complement and extend the findings reported here.

Experimental Section

General Methods. $\mathbf{Bn_2}$**-L**, $[Re(bpy)(CO)_3(\mathbf{Bn_2\text{-}L})][PF_6]$, and $[Re(bpy)(CO)_3(\mathbf{H_2\text{-}L})][PF_6]$ were synthesized as described previously,[23] with minor modifications, most notably the increase of the hydrogen pressure to 3.5 bar to ensure complete deprotection of $[Re(bpy)(CO)_3(\mathbf{Bn_2\text{-}L})](PF_6)$ to $[Re(bpy)(CO)_3(\mathbf{H_2\text{-}L})](PF_6)$.

Commercially available reagents and solvents were obtained from Aldrich and Fluka and used as supplied. Solvents were dried over molecular sieves where required. NMR spectra were recorded on a Bruker AMX500 instrument (^{1}H at 500.13 MHz, ^{13}C at 125.76 MHz). Electrospray ionization (ESI) mass spectra were recorded on a Bruker microTOF electrospray mass spectrometer or a ThermoFinnigan LCQ-Classic instrument. UV/vis spectra were measured on an Agilent 8453 spectrophotometer in 10 mm quartz cuvettes. Uncorrected emission and excitation spectra were recorded on a Hitachi F-4500 fluorimeter, equipped with a red-sensitive R928F photomultiplier tube, in four-windowed 10 mm quartz cuvettes. IR spectra were recorded on a Unicam-Mattson RS-FTIR spectrometer.

Synthesis of $\mathbf{Me_2}$**-L.** 2, 3-Dimethoxybenzoic acid (3.62 g, 20 mmol) was dissolved in dry dimethylformamide (DMF, 150 mL) and combined with triethylamine (5.575 mL, 40 mmol), DMAP (0.489 g, 4 mmol) and *p*-nitrobenzenesulfonyl chloride (4.390 g, 20 mmol). The reaction mixture was stirred for 20 min before being cooled to 0 °C in an ice bath. A solution of 4-aminopyridine (2.061 g, 22 mmol) in dry DMF (50 mL) was then added slowly to the reaction mixture. The resulting orange solution was stirred overnight at room temperature to ensure completion of the reaction. The solution was then filtered to remove triethyl ammonium chloride. After removal of the DMF, the remaining residue was extracted 3 times with CH_2Cl_2 (50 mL). The combined organic fractions were washed, alternately with saturated sodium hydrogen carbonate solution and distilled water, a total of 3 times. Finally, the resulting organic phase was dried over magnesium sulfate. Removal of the solvent yields the crude product, which was recrystallized from CH_2Cl_2-hexane. Yield: 4.75 g (18.4 mmol, 92%).

IR (KBr), ν (cm^{-1}): 3305 (s, br, ν_{NH}); 3013 (m); 2936 (w); 1693 (s, ν_{CO}); 1581 (s). ^{1}H NMR, (500 MHz, $CDCl_3$) δ [ppm]: 10.29 (1H, s, N−H); 8.57 (2H, d, J = 5.5 Hz, H^a, H$^{a'}$); 7.79 (1H, dd, J = 8.0, 1.5 Hz, H^f); 7.67 (2H, d, J = 6.0 Hz, H^b, H$^{b'}$); 7.26 (1H, t, J = 8.0 Hz, H^g); 7.17 (1H, dd, J = 8.0, 1.5 Hz, H^h); 4.05 (3H, s, OMe); 3.97 (3H, s, OMe). ^{13}C NMR, (500 MHz, $CDCl_3$) δ [ppm]: 163.8 (C=O); 152.6 (C^d); 150.1 (C^a, C$^{a'}$); 147.4 (C^j); 145.7 (C^i); 125.8; 125.0; 123.0; 116.5; 114.1 (C^b, C$^{b'}$); 61.8 (OMe); 56.2 (OMe). EI-MS: m/z = 259 (100%, $[M+H]^+$). HRMS Calc. for $C_{14}H_{15}N_2O_3$, 259.2852. Found $[M+H]^+$, 259.2854 (difference 0.2 mDa).

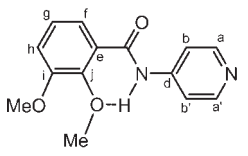

$\mathbf{Me_2}$**-L**

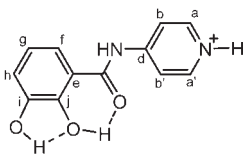

$[\mathbf{H_3}$**-L**$]^+$

Synthesis of $[\mathbf{H_3}$**-L**$]$**Br.** Under an inert atmosphere, a solution of $\mathbf{Me_2}$**-L** (0.5 g, 1.94 mmol) in dry CH_2Cl_2 (25 mL) was cooled to 0 °C. A solution of BBr_3 in CH_2Cl_2 (1 M, 10.75 mL) was added dropwise. The resulting yellow suspension was stirred at room temperature overnight. Water (8.60 mL) was added carefully at 0 °C (HBr evolution), and the mixture was stirred for 2 h to ensure complete hydrolysis. The precipitate was then filtered off and washed with water. The resulting solid was dissolved in methanol and evaporated three times to remove boron compounds. Finally, the residue was dissolved in methanol, the resulting solution was acidified with HBr, and the product precipitated by addition of diethyl ether. Yield: 0.39 g (1.25 mmol, 64%).

IR (KBr), ν (cm^{-1}): 3463 (m, $\nu_{O-H/N-H}$); 3372 (m, $\nu_{O-H/N-H}$); 3253 (s, br, $\nu_{O-H/N-H}$); 1665 (s, $\nu_{C=O}$); 1506 (m); 1331; 1223. ^{1}H NMR, (500 MHz, CD_3OD) δ: 8.66 (2H, d, J = 6.0 Hz, H^a, H$^{a'}$); 8.33 (2H, d, J = 6.0 Hz, H^b, H$^{b'}$); 7.50 (1H, d, J = 8.0 Hz, H^f); 7.09 (1H, d, J = 7.5 Hz H^h); 6.89 (1H, t, J = 8.0 Hz, H^g). ^{13}C NMR, (500 MHz, CD_3OD) δ: 168.0 (C=O); 153.1 (C^d); 147.3 (C^j); 146.1 (C^i); 142.5 (C^a, C$^{a'}$); 119.7, 119.6; 117.0; 115.3 (C^b, C$^{b'}$). ESI-MS: m/z = 231 (100%, $[M+H]^+$). HRMS Calc. for $C_{12}H_{11}N_2O_3$, 231.0764. Found $[M]^+$, 231.0766 (difference 0.2 mDa). Elemental Analysis: found C, 43.85; H, 3.99; N, 8.48%. Required for $C_{12}H_{11}N_2O_3Br \times 1\ H_2O$: C, 43.80; H, 3.98; N, 8.51%.

Synthesis of $[\mathbf{MoO_2}\{\mathbf{Re(bpy)(CO)_3(L)}\}_\mathbf{2}]$**.** $[Re(bpy)(CO)_3(\mathbf{H_2\text{-}L})]PF_6$ (10 mg, 0.01 mmol) was dissolved in the minimum

(33) Kuimova, M. K.; Alsindi, W. Z.; Dyer, J.; Grills, D. C.; Jina, O. S.; Matoušek, P.; Parker, A. W.; Portius, P.; Sun, X. Z.; Towrie, M.; Wilson, C.; Yang, J. X.; George, M. W. *Dalton Trans.* **2003**, 3996.
(34) Busby, M.; Matoušek, P.; Towrie, M.; Vlček, A. *J. Phys. Chem. A* **2005**, *109*, 3000.
(35) Schoonover, J. R.; Strouse, G. F. *Chem. Rev.* **1998**, *98*, 1335.
(36) Gabrielsson, A.; Hartl, F.; Zhang, H.; Lindsay Smith, J. R.; Towrie, M.; Vlček, A.; Perutz, R. N. *J. Am. Chem. Soc.* **2006**, *128*, 4253.
(37) Vlček, A. *Top. Organomet. Chem.* **2010**, *29*, 73.

amount of a solvent system consisting of a 2:1 acetonitrile/water mixture, and the pH of the solution was adjusted to 3 with dilute hydrochloric acid. Five microliters of an aqueous solution of sodium molybdate dihydrate (242 mg, 1 mmol dissolved in 1 mL water) were added to obtain a 2:1 ratio of sensor to molybdate. Equilibration of the mixture resulted in an increase of the pH to 6. Crystals suitable for single X-ray diffraction were obtained after 6 h. Yield: 3.4 mg (0.002 mmol, 47%).

IR (KBr), ν (cm^{-1}) (CO): 2029(s), 1925 (s). ^{1}H NMR: (500 MHz, DMF-d_7): δ: 9.48 (dd, 4 H, H^a, $H^{a'}$); 8.85 (dd, 4 H, H^d, $H^{d'}$); 8.52 (dt, 4 H, H^c, $H^{c'}$); 6.99 (d, 4 H, H^f, $H^{f'}$); 6.76 (d, 2 H, H^g); 6.57 (d, 2 H, H^i); 6.11 (t, 2 H, H^h). $T = -40$ °C: 8.19 (d, 4 H, H^e, $H^{e'}$), 8.14 (t, 4 H, H^b, $H^{b'}$). ESI-MS: m/z = 1461 (100%, $[M+Na]^+$ for ^{187}Re and ^{96} Mo). Elemental Analysis: found C, 37.82; H, 2.99; N, 7.08%. Required for $C_{50}H_{32}N_8O_{14}Mo_1Re_2 \times 9\ H_2O$: C, 37.55; H, 3.15; N, 7.01%.

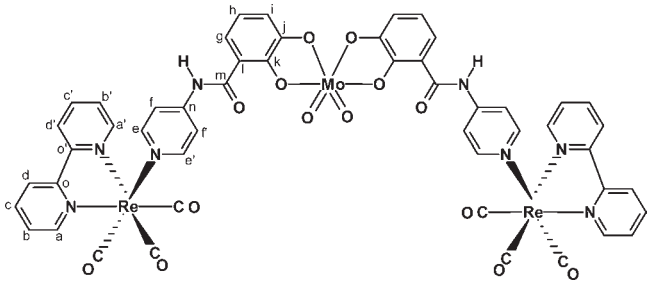

X-ray Crystallography. Diffraction data were collected using a Bruker Smart Apex X-ray diffractometer with an Oxford cryostream cooling system and Mo−K_α radiation source (λ = 0.71073 Å) using a SMART CCD camera. The structure was solved by direct methods using SHELXS-97 and refined by full-matrix least-squares using SHELXL-97 (G. M. Sheldrick, University of Göttingen, Germany, **1997**). Crystal data and refinement details are summarized in Table 1. The crystal contained seven water molecules two of which were disordered and modeled with 50% occupancy over two sites. The hydrogen atoms of the water molecules could not be located by difference map and so were omitted. CCDC 799865 contains the crystallographic data, which can be obtained free of charge from The Cambridge Crystallographic Data Centre via www.ccdc.cam.ac.uk.

General pH Titration Procedures. (a). Absorption, Excitation, and Emission Studies. Unless otherwise stated, the following general conditions apply. All titrations were carried out in air at room temperature using either aqueous acetonitrile (5% v/v water) or aqueous DMF (5% v/v water) as solvent, depending on the solubility of the compound under investigation. Adjustments to the pH were made with 0.6 mM $[Me_4N]OH$ in water and 0.6 mM HCl or HBr in the respective solvent system, as indicated. The absorption, excitation, and emission spectra were recorded in 10 mm quartz cuvettes after equilibration. Excitation and emission spectra are uncorrected. pH values were determined using a WTW Profilab pH 597 pH meter with a Mettler Toledo Inlab 422 electrode and are given as measured in the respective solvent system.

(b). Mass Spectrometry. A solution containing 1 equiv of potassium molybdate (0.79 mM) and 2 equiv of $[Re(bpy)(CO)_3(\mathbf{H_2}\text{-}\mathbf{L})]^+$ (1.58 mM) in aqueous DMF (5% water) was prepared. After equilibration, the pH value was measured and the ESI-MS was recorded on a ThermoFinnigan LCQ-Classic instrument.

Transient Absorption Spectroscopy. The measurements were carried out in the Department of Photochemistry and Molecular Science at Uppsala University. The concentration of the samples was 0.017 mM in DMF/water 20:1 (v/v). The pH was adjusted by addition of HCl and $[Bu_4N]OH$. The samples were measured first in unbuffered solutions in the presence and absence of oxygen. However, the pH was seen to increase upon laser exposure. The samples were subsequently buffered with 2, 4-lutidine and the measurements were repeated. A comparison of the pH values and absorption spectra recorded before and after the measurements confirmed that the buffer prevented the pH from drifting and that no significant photodecomposition had occurred.

Femtosecond transient absorption spectra were recorded using an amplified 1 kHz system. Briefly, 800 nm pulses (80 fs, 1 kHz) were generated in a Coherent Vitesse/Legend-HE system. The 800 nm light was split into pump and probe pulses. Pump light (≈100 fs, 355 nm, ≈300 nJ per pulse) was obtained using a Light Conversion TOPAS set to 710 nm and an external BBO doubling crystal. Broadband probe light (≈100 fs) was generated in a 3 mm thick CaF_2 plate, and residual 800 nm light was attenuated using a KG3 filter. The polarization of the pump light was set to 55° relative to that of the probe light using a waveplate. Full spectra were detected using a diode array (Pascher Instruments, Lund, Sweden) for each laser pulse. The reported spectra and kinetic traces are averages of 5000 to 10000 shots. All measurements were done in 1 mm path length cuvettes, which were oscillated to avoid photobleaching and accumulation of degradation products. The femtosecond transient absorption data were fitted using iterative reconvolution of exponential functions with a Gaussian response (200−300 fs) using the Igor Pro (Wavemetrics, Lake Oswego, OR, U.S.A.) software package. Spectra are not chirp-corrected, as the chirp was found to be insignificant at the time scales reported. Nonlinear effects within the pulse width (< 300 fs) were either fitted using a dummy lifetime of 5 fs or removed using visual inspection.

Table 1. Crystal Data and Summary of Data Collection and Refinement Details for $[MoO_2\{Re(bpy)(CO)_3(L)\}_2]\cdot CH_3CN\cdot 7(O)$

empirical formula	$C_{52}H_{35}MoN_9O_{21}Re_2$
formula weight	1590.23
temperature	100(2) K
wavelength	0.71073 Å
crystal system	triclinic
space group	$P\bar{1}$
unit cell dimensions	a = 13.3454(14) Å b = 15.1335(16) Å c = 16.1209(17) Å α = 104.903(2)° β = 113.199(2)° γ = 92.983(3)°
V	2848.5(5) Å^3
Z	2
density (calculated)	1.854 Mg/m^3
absorption coefficient	4.541 mm^{-1}
F(000)	1540
crystal size	0.11 × 0.04 × 0.04 mm^3
θ range for data collection	1.41 to 23.54°.
index ranges	$-14 \le h \le 14$ $-16 \le k \le 15$ $-17 \le l \le 18$
reflections collected	14029
independent reflections	8379 [R(int) = 0.0598]
completeness to θ = 23.54°	98.9%
absorption correction	semiempirical from equivalents
max. and min transmission	0.830 and 0.631
refinement method	full-matrix least-squares on F^2
data/restraints/parameters	8379/12/785
goodness-of-fit on F^2	0.978
final R indices [$I > 2\sigma(I)$]	R1 = 0.0548, wR2 = 0.1189
R indices (all data)	R1 = 0.1001, wR2 = 0.1319
largest diff. peak and hole	2.387 and −1.512 e Å^{-3}

Results and Discussion

Synthesis and Characterization. $Re(bpy)(CO)_3(\mathbf{Bn_2}\text{-}\mathbf{L})](PF_6)$ was synthesized as described previously[23] and

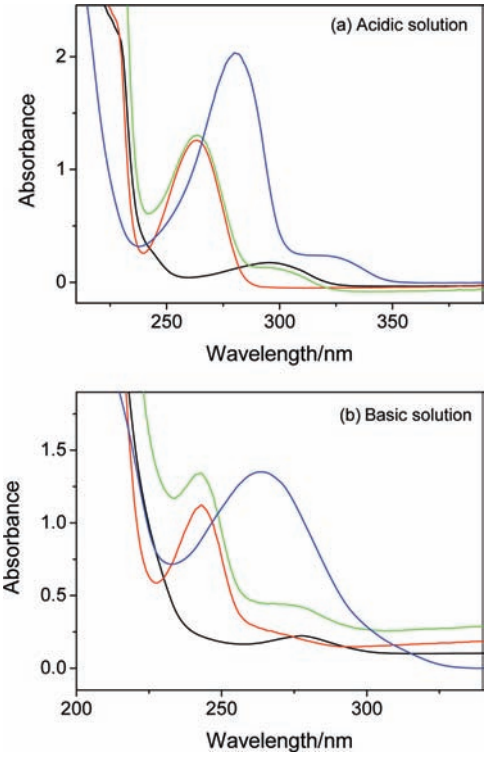

Figure 1. Comparison of the absorption spectra of 0.1 mM solutions of 2, 3-dimethoxybenzoic acid (black), 4-aminopyridine (red) and the resulting summation spectrum (green) with the spectrum of the methyl-protected ligand (blue) in aqueous acetonitrile (5% water) under (a) acidic and (b) basic conditions.

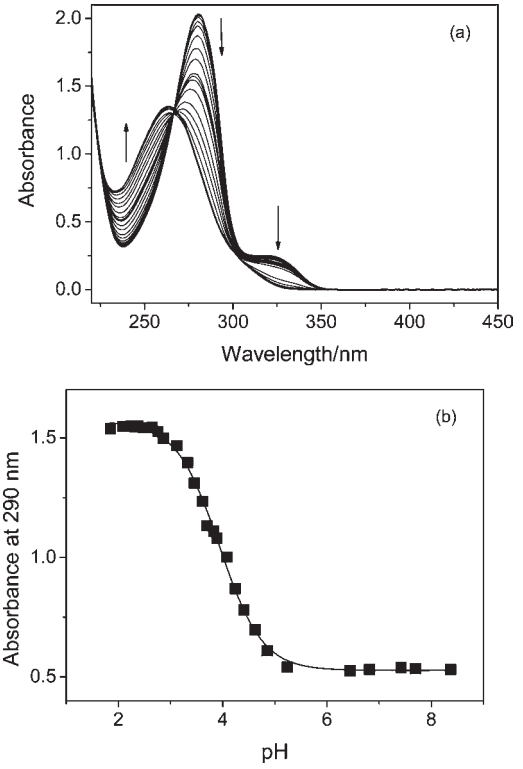

Figure 2. (a) Absorption spectra recorded between pH 1.8 and 8.4 during the titration of an acidic solution (0.1 mM) of **Me_2-L** in aqueous acetonitrile (5% water) with $[Me_4N]OH$. (b) Plot of the absorbance at 290 nm as a function of pH.

complete debenzylation was achieved by catalytic hydrogenolysis (3.5 bar H_2, 5% Pd on charcoal) to yield $[Re(bpy)(CO)_3(\mathbf{H_2\text{-}L})](PF_6)$.

To obtain the Mo(VI) complex, $[Re(bpy)(CO)_3(\mathbf{H_2\text{-}L})]PF_6$ (0.01 mmol) was dissolved in the minimum amount of a solvent system consisting of a 2:1 acetonitrile/water mixture, and the pH of the solution was adjusted to 3 with dilute hydrochloric acid. Five microliters of an aqueous solution of sodium molybdate dihydrate (1 mmol dissolved in 1 mL water) were added to obtain a 2:1 ratio of sensor to molybdate. Equilibration of the mixture resulted in an increase of the pH to 6 and the crystallization of the dioxo-Mo(VI) complex, which was isolated and characterized by IR and proton NMR spectroscopy, ESI mass spectrometry, and X-ray crystallography.

Me_2-L was synthesized by reacting commercially available 2, 3-dimethoxybenzoic acid with 4-aminopyridine. The downfield shift of the NH proton (δ 10.29) indicates hydrogen bonding to the adjacent methoxy-oxygen. **Me_2-L** was demethylated with BBr_3 to give the free ligand **[H_3-L]Br**, which was characterized by mass spectrometry, elemental analysis, IR spectroscopy, and NMR spectroscopy. The values of the ν(OH) bands in the IR spectra are suggestive of intramolecular hydrogen bonding interactions, as indicated in Scheme 1.

Spectroscopic Properties. 1. UV/vis Absorption Spectra of Me_2-L and [H_3-L]Br. The pH-dependence of the electronic absorption spectra of **Me_2-L** and **[H_3-L]Br** was investigated in a mixed solvent system consisting of 5% water in acetonitrile. The spectra of the starting materials 2, 3-dimethoxybenzoic acid and 4-aminopyridine were recorded for comparison. All pH values are given as measured by standard glass electrode in the solvent system used.

Figure 1a shows the absorption spectra of **HMe_2-L$^+$** and **Me_2-L** in comparison with the absorption spectra of equimolar acidic solutions of the two starting materials 2, 3-dimethoxybenzoic acid and 4-aminopyridine and the sum of their spectra. The corresponding spectra for basic solutions are shown in Figure 1b. It is evident that the absorbance in the region between 225 and 350 nm is mainly dominated by transitions associated with the pyridine-moiety of the ligand, with some contributions from catecholamide-based transitions. Under both conditions, the most intense band observed in the spectrum of the methyl-protected ligand is broader and clearly red-shifted, the latter indicating a decrease in the HOMO −LUMO gap. In addition, the absorbance of the main band increases significantly in acidic solution if compared to the summation spectrum, providing additional evidence for an increase in the degree of conjugation.

The absorption spectral changes associated with the deprotonation of the pyridinium-unit in **[HMe_2-L]Br** were investigated in more detail by titration of an acidic solution with small aliquots of base (Figure 2, top). The pH-dependence of the absorbance at 290 nm indicates only one step, the deprotonation of the pyridinium unit and formation of **Me_2-L**. Upon deprotonation, the absorption maximum shifts to higher energy, from 280 to 263 nm, as observed in similar pyridine-derivatives.[38] The

(38) Cattaneo, M.; Fagalde, F.; Katz, N. E. *Inorg. Chem.* **2006**, *45*, 6884.

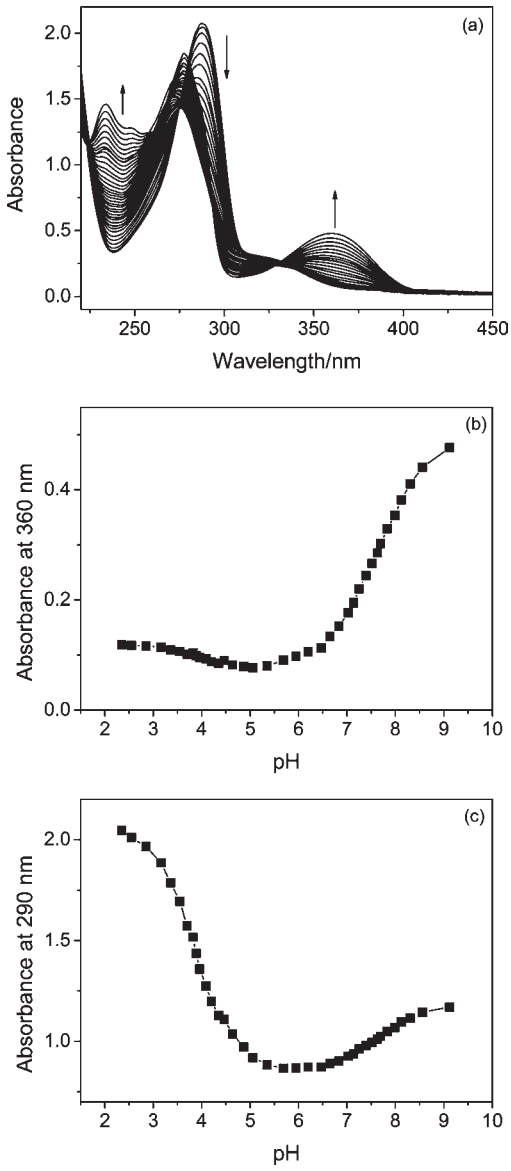

Figure 3. (a) Absorption spectra recorded between pH 2.3 and 9.1 during the titration of an acidic solution (0.065 mM) of $\mathbf{H_3\text{-}L}^+$ in aqueous acetonitrile (5% water) with $[Me_4N]OH$. (b) Plot of the absorbance at 360 nm as a function of pH. (c) Plot of the absorbance at 290 nm as a function of pH.

sigmoidal decrease of the absorbance at 290 nm is centered at around pH 3.9 (Figure 2b).

Subsequently, the absorption spectra of the ligand $\mathbf{H_2\text{-}L}$ were recorded at a range of pH values (Figure 3a). The titration of an acidic solution of $[\mathbf{H_3\text{-}L}]^+$ with base revealed two deprotonation steps, the formation of $\mathbf{H_2\text{-}L}$ followed by the formation of $\mathbf{H\text{-}L}^-$. The increase of the lower energy absorption at around 360 nm above pH 6 reflects the second step, the deprotonation of the dihydroxybenzamide-unit of the ligand to give $\mathbf{H\text{-}L}^-$ (Figure 3b). The midpoint of the sigmoidal increase is located at pH 7.6, which is slightly lower than corresponding pK_a value for *N, N′*-dimethyl-2, 3-dihydroxybenzamide, which was reported as 8.42 in water.[39] An

(39) Harris, W. R.; Carrano, C. J.; Cooper, S. R.; Sofen, S. R.; Avdeef, A. E.; McArdle, J. V.; Raymond, K. N. *J. Am. Chem. Soc.* **1979**, *101*, 6097.

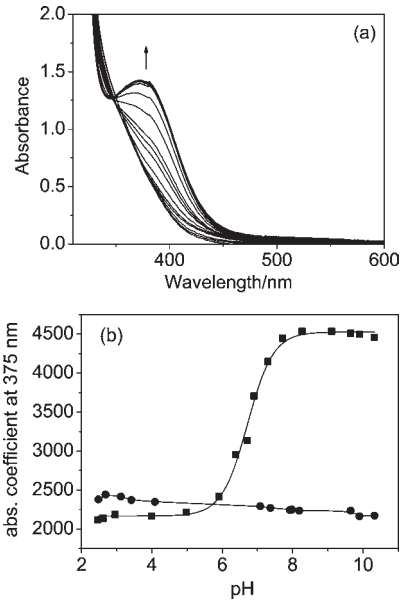

Figure 4. (a) Absorption spectra of $[Re(bpy)(CO)_3(\mathbf{H_2\text{-}L})]^+$ recorded between pH 2.5 and 10.3 during the titration of acidic solutions in aqueous DMF with $[Me_4N]OH$. (b) Plot of the molar absorption coefficient at 375 nm of $[Re(bpy)(CO)_3(\mathbf{H_2\text{-}L})]^+$ (squares, 0.3 mM) and $[Re(bpy)(CO)_3(\mathbf{Bn_2\text{-}L})]^+$, (circles, 0.26 mM) as a function of pH.

increase in acidity, however, is consistent with the structural differences, in particular the electron withdrawing effect of the pyridine-unit in $\mathbf{H\text{-}L}^-$ as opposed to the electron-donating properties of the two *N*-methyl-substituents in *N, N′*-dimethyl-2, 3-dihydroxybenzamide.

The intense absorption bands with maxima at 277 nm (pH 9.1) and 290 nm (pH 2.3) are due to overlapping pyridine- and dihydroxybenzamide-based transitions. Accordingly, the plot of the absorbance at 290 nm versus pH reveals both the deprotonation of the pyridinium-unit to give $\mathbf{H_2\text{-}L}$ (with midpoint at pH 3.9) and the deprotonation of the dihydroxybenzamide-unit to give $\mathbf{H\text{-}L}^-$ (with midpoint at pH 7.6, Figure 3c). The former agrees well the midpoint obtained for the deprotonation of $[\mathbf{HMe_2\text{-}L}]^+$, indicating that the methylation of the catechol-unit has no significant impact on the pK_a value of the pyridine-unit.

The above assignment of the two protonation sites was confirmed by ^{1}H NMR spectroscopy (Figure S1, Supporting Information). The ^{1}H NMR spectrum of $\mathbf{H_2\text{-}L}$ shows two doublets at 8.48 and 7.85 ppm for the protons of the pyridine-unit and three resonances at 7.49, 7.04, and 6.85 ppm for the protons of the catechol unit. Addition of base and formation of $\mathbf{H\text{-}L}^-$ results in a significant upfield shift of two of the resonances due to the catechol-protons to 6.40 and 6.82 ppm, which is consistent with the deprotonation of the 2-hydroxy-position. In contrast, the pyridine resonances barely shift upon addition of base. On the other hand, the addition of HBr and formation of $[\mathbf{H_3\text{-}L}]\mathbf{Br}$ does not affect the catechol-dominated area of the spectrum, but results in a marked downfield shift of the two doublets due to the pyridine protons to 8.69 and 8.39 ppm. This is consistent with the protonation of the pyridine-unit.

UV/vis Absorption Spectra of $[Re(bpy)(CO)_3(\mathbf{Bn_2\text{-}L})]^+$ and $[Re(bpy)(CO)_3(\mathbf{H_2\text{-}L})]^+$. The pH-dependence of the electronic absorption spectra of $[Re(bpy)(CO)_3(\mathbf{Bn_2\text{-}L})]^+$

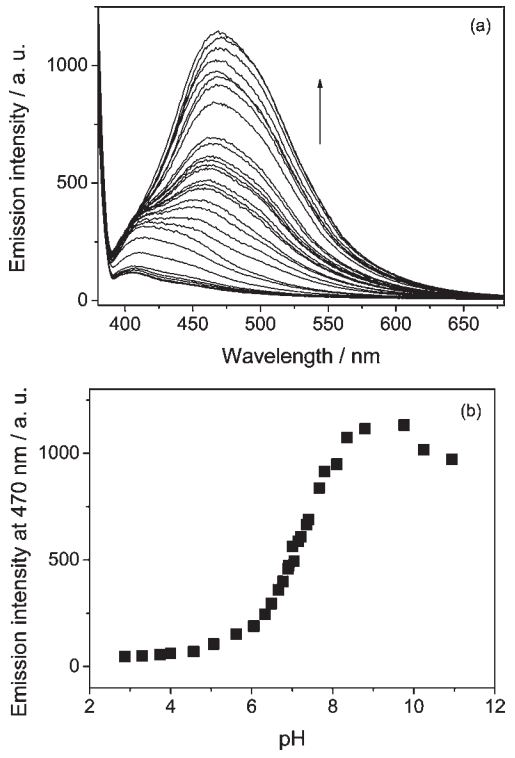

Figure 5. (a) Emission spectra (λ_{exc} = 360 nm) recorded during the titration of an acidic 0.1 mM solution of ligand $\mathbf{H_2}$-**L** in aqueous acetonitrile with $[Me_4N]OH$. (b) pH dependence of the emission intensity at 470 nm, λ_{exc} = 360 nm.

and $[Re(bpy)(CO)_3(\mathbf{H_2}\text{-}\mathbf{L})]^+$ was investigated in aqueous DMF (5% water). In the absorption spectrum of the benzyl-protected complex $[Re(bpy)(CO)_3(\mathbf{Bn_2}\text{-}\mathbf{L})]^+$, the lowest energy band (shoulder at ca. 375 nm) can be assigned to a Re(dπ)→bpy charge transfer (MLCT) transition by reference to the spectra of similar complexes.[8] In agreement with this assignment, the absorption spectra of $[Re(bpy)(CO)_3(\mathbf{Bn_2}\text{-}\mathbf{L})]^+$ change only very little with pH (Figure S2, Supporting Information).

In contrast, the titration of an acidic solution of the deprotected sensor $[Re(bpy)(CO)_3(\mathbf{H_2}\text{-}\mathbf{L})]^+$ with base leads to an increase in the absorbance at 375 nm with pH (Figure 4a), indicating an overlap of the pH-independent MLCT band with pH-dependent ligand-based transitions. At high pH, a band emerges at 380 nm, which may be attributed to the deprotonation of the corresponding OH-group of the dihydroxybenzamide-unit of the sensor. From the inflection point, a pK_a-value of 6.7 can be estimated (Figure 4b).

The pK_a value of 6.7 obtained for $[Re(bpy)(CO)_3(\mathbf{H_2}\text{-}\mathbf{L})]^+$ is lower than the corresponding pK_a value of 7.6 obtained for $\mathbf{H_2}$-**L**, but the trend is consistent with the electron withdrawing effect of the electron poor, rhenium-coordinated pyridine unit in $[Re(bpy)(CO)_3(\mathbf{H_2}\text{-}\mathbf{L})]^+$. It should also be considered that solubility limitations required the titrations of $[Re(bpy)(CO)_3(\mathbf{Bn_2}\text{-}\mathbf{L})]^+$ and $[Re(bpy)(CO)_3(\mathbf{H_2}\text{-}\mathbf{L})]^+$ to be performed in aqueous DMF, while the ligand was investigated in aqueous acetonitrile. The pK_a values obtained are therefore not directly comparable. Nevertheless, the ligand spectra obtained are consistent with the conclusion that the pH-dependence of the low-energy band in the spectra of

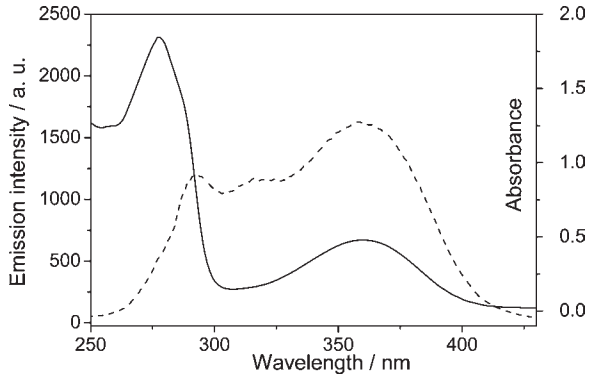

Figure 6. Excitation spectrum of $\mathbf{H\text{-}L}^-$ monitored at 470 nm (dashed line, 0.02 mM, pH 11) in comparison with the absorption spectrum (solid line, 0.065 mM, pH 9).

$[Re(bpy)(CO)_3(\mathbf{H_2}\text{-}\mathbf{L})]^+$ is due to the deprotonation of the dihydroxybenzamide-unit.

For both $[Re(bpy)(CO)_3(\mathbf{H}\text{-}\mathbf{L})]$ and $\mathbf{H\text{-}L}^-$ the back-titration with acid restored the original absorption spectra, confirming that the catecholate unit is not oxidized during the titration.

2. Emission Behavior of $[\mathbf{H_3}\text{-}\mathbf{L}]$Br. Acidic solutions of $\mathbf{H_3\text{-}L}^+$ in aqueous acetonitrile are not emissive below pH 3. At pH 4, weak emission with maximum at 405 nm is observed upon excitation into the catecholate-dominated absorption band at around 360 nm. Further increase of the pH leads to an increase of the emission intensity up to a pH value of 9, with a shift of the maximum to 470 nm (Figure 5a). A sigmoidal fit of the corresponding pH profile gives a midpoint of 7.5 (Figure 5b). The midpoint of 7.5 is very similar to the second pK_a value of 7.6 obtained from the electronic absorption spectra, suggesting that the increase in emission intensity is due to the deprotonation of the OH-group in the 2-position of the catecholamide-unit and formation of $\mathbf{H\text{-}L}^-$. This conclusion was further confirmed by the excitation spectrum recorded at pH 11, monitoring the emission intensity at 470 nm (Figure 6). The low energy region in the excitation spectrum of $\mathbf{H\text{-}L}^-$ shows a band that matches the absorption band of the deprotonated catecholamide-unit, confirming that the emission observed at 470 nm is due to the excitation of catecholamide-based transitions. Further addition of base leads to a decrease in emission intensity, which may be due to the deprotonation of the OH-group in the 3-position of the dihydroxybenzamide-unit.

The absorption band at 360 nm and the emission band at 470 nm of $\mathbf{H\text{-}L}^-$ are likely to be associated with the same electronic excited state. The observation that these low energy transitions are unique to the deprotonated form together with the solvent dependence[40] of the emission leads us to assign the excited state as intramolecular charge transfer state, in which the catecholate acts as the donor and the pyridylamide as the acceptor.[41]

Since the optimal excitation wavelength for the molybdate sensor (370 nm) falls into the wavelength range affected by the intramolecular charge transfer absorption of $\mathbf{H\text{-}L}^-$, ligand-based electronic transitions might play a

(40) In chloroform, the emission maximum is located at 445 nm, whilst in water, the fluorescence is quenched.

(41) Aronica, C.; Venancio-Marques, A.; Chauvin, J.; Robert, V.; Lemercier, G. *Chem.—Eur. J.* **2009**, *15*, 5047.

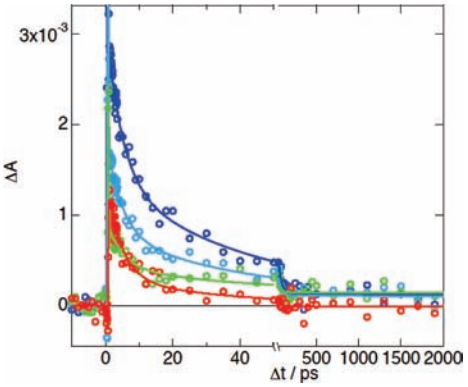

Figure 7. Kinetic traces obtained from the transient absorption spectra of $\mathbf{H_3\text{-}L}^+$ at pH 3.7 at a selection of wavelengths (dark blue 420 nm, light blue 470 nm, green 550 nm, red 630 nm. Solid lines are best multicomponent fits to three lifetimes. Nonlinear effects within the pulse width have been accounted for by the addition of a 5 fs lifetime. The *x*-axis contains two scales, as indicated by the axis break).

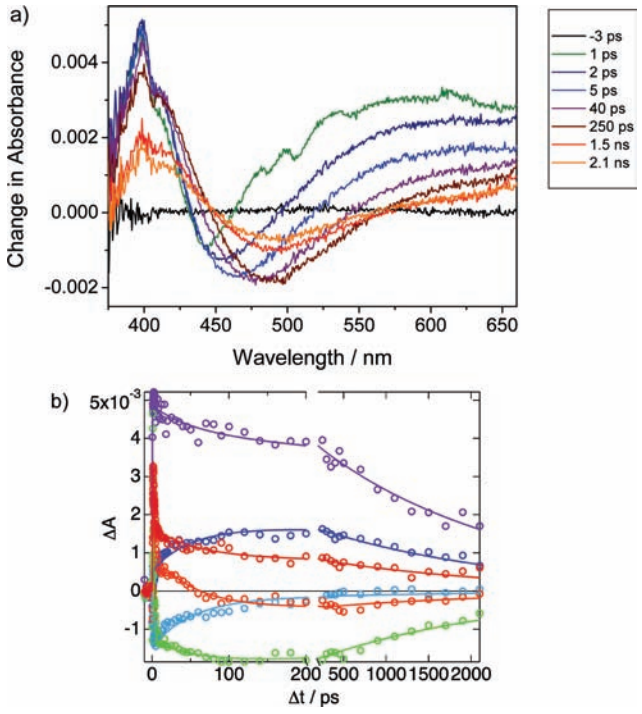

Figure 8. (a) Transient absorption/emission spectra of $\mathbf{HL}^-$ obtained at pH 7.9 after the indicated time intervals. (b) Kinetic traces at a selection of wavelengths (violet 400 nm, dark blue 430 nm, light blue 450 nm, green 495 nm, orange 550 nm, red 630 nm. Solid lines are best fits to two lifetimes. Nonlinear effects within the pulse width have been removed. The *X*-axis contains two scales, as indicated by the axis break).

role in the signaling mechanism. The photophysical properties of ligand $\mathbf{H_2\text{-}L}$ were therefore studied further by ultrafast transient absorption spectroscopy on a 0.1 ps to 2.1 ns time scale with laser excitation at 355 nm.

The transient spectra recorded in aqueous DMF (5% water) at pH 3.7 are characterized through absorption bands with maxima at 398 and 420 nm (Figure S3, Supporting Information). A multicomponent fit of the decay profiles at a selection of wavelengths gives lifetimes of 5 and 40 ps (Figure 7).

Upon increase of the pH to 7.9 an absorption band with maximum at 398 nm is observed almost immediately after the excitation pulse. The transient absorption then decays without significant shift in the band position (Figure 8a). Since there is virtually no ground state absorption above 410 nm at this pH, the negative signal observed between 425 and 560 nm is caused by stimulated emission of the sample rather than bleaching of the ground state. Initially, the minimum of the negative signal is located at 440 nm, but the position of the band then red-shifts to about 490 nm. By comparison with the fluorescence spectra (Figure 5a) it is evident that fluorescence from the relaxed excited state is significant up to 650 nm. Therefore it is most probable that the decrease in net absorption to the red (Figure 8) is due to a dynamic Stokes shift of the stimulated emission and not due to a decrease in the excited state absorption. Excited state absorption above 500 nm is present both at high pH and at low pH also at low pH (Figure 7 and Supporting Information, Figure S3). At low pH all traces have positive amplitudes. What is absent at pH = 3.7 is clear stimulated emission, which is in agreement with the weak fluorescence at this pH (Figure 5b).

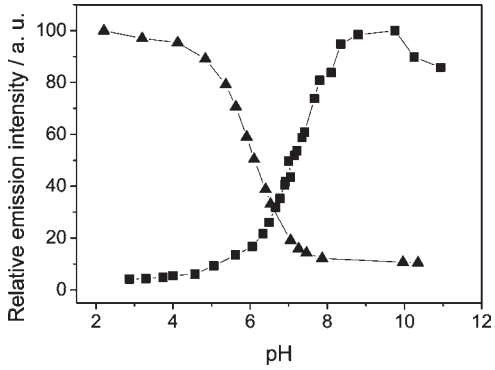

Figure 9. pH dependence of the relative emission intensity of a 0.1 mM solution of $[Re(bpy)(CO)_3(\mathbf{H_2\text{-}L})]^+$ (triangles, λ_{exc} = 370 nm, λ_{em} = 565 nm) and a 0.1 mM solution of $\mathbf{H_2\text{-}L}$ (squares: λ_{exc} = 360 nm, λ_{em} = 470 nm) in aqueous acetonitrile (5% water).

A three-exponential fit of the decay profile gives lifetimes of 1.4, 60, and approximately 2200 ps (Figure 8b). The spectral envelope does not appear to change much with time except for the apparent red-shift of the emission. The wavelength of the emission maximum at $t > 100$ ps agrees well with that observed by steady state fluorescence measurements. Although the exact origin of the lifetimes cannot be determined, it is conceivable that the two short lifetimes correspond to internal molecular and external solvent relaxation, especially when considering the relatively high viscosity of the solvent system used.

3. Comparison with the Emission Properties of the Molybdate Sensor $[Re(bpy)(CO)_3(\mathbf{H_2\text{-}L})]^+$. In contrast to the emission properties of $\mathbf{H_2\text{-}L}$, the pH profile of the emission of the molybdate sensor $[Re(bpy)(CO)_3(\mathbf{H_2\text{-}L})](PF_6)$ shows a decrease in emission intensity upon deprotonation. In acidic solution, the excitation at 370 nm gives rise to emission from the ^{3}MLCT state at around 565 nm, as previously reported.[23] The intensity of the emission decreases sigmoidally with increasing pH. In aqueous acetonitrile, the inflection point is located at pH 5.9, if the pH scale is uncorrected for the composition of the solvent system used[42] (Figure 9).

(42) The inflection point of 4.9 reported in our previous paper[23] was obtained by applying a correction of −1 to the measured value of 5.9 to account for the effect of the aqueous acetonitrile solvent mixture used.

Table 2. Selected Spectroscopic Data and Protonation Constants for the Protected Ligand, Deprotected Ligand and the Sensor Molecule[a]

	$\mathbf{Me_2}$-LH$^+$	$\mathbf{Me_2}$-L	$\mathbf{H_3}$-L$^+$	$\mathbf{H_2}$-L	HL$^-$	[Re(bpy)(CO)$_3$($\mathbf{H_2}$-L)]$^+$	[Re(bpy)(CO)$_3$(H-L)]
absorption λ_{max}/nm	280	263	286	~274	278, 360	shoulder	375[c]
emission							
λ_{em}/nm			405 weak	~460	470	565	565 weak
(λ_{ex}/nm)			(360)	(360)	(360)	(370)	(370)
pK_a	3.9		3.9		7.6	6.7[c]	
pH$_i$[b]					7.5	5.9	

[a] Aerated solutions at room temperature in aqueous acetonitrile (5% water). [b] pH$_i$ is the pH at the inflection point of the fluorescence titration curve. [c] Determined in aqueous DMF (5% water).

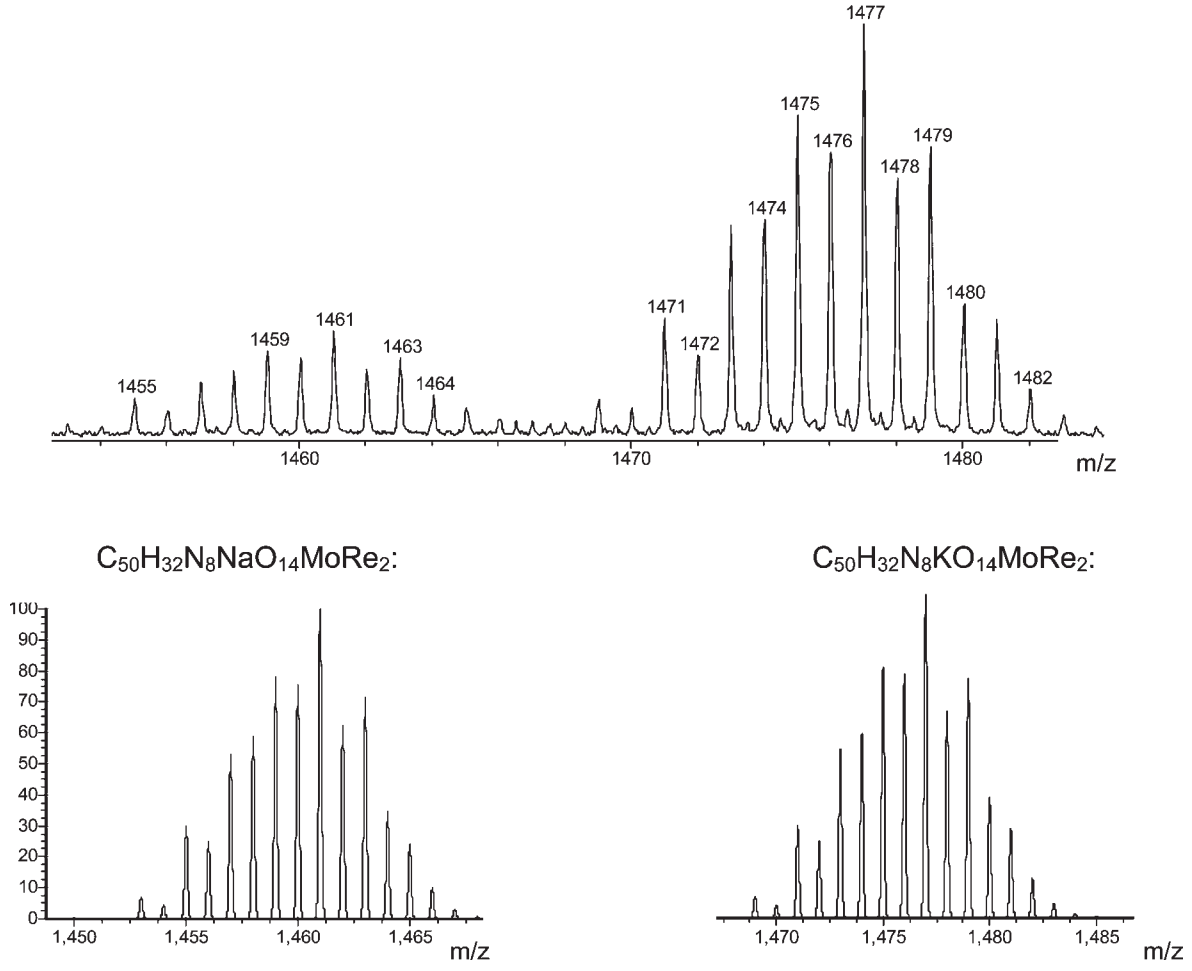

Figure 10. Top: Positive mode ESI mass spectrum of a reaction mixture containing 2 equiv of [Re(bpy)(CO)$_3$($\mathbf{H_2}$-L)]$^+$ and 1 equiv of molybdate in aqueous DMF (5% water) at pH 10. Bottom: Isotopic distribution pattern calculated for the sodium (left) and potassium (right) adducts of [MoO$_2${Re(bpy)(CO)$_3$(L)}$_2$].

Table 2 compares the spectroscopic characteristics previously obtained[23] for [Re(bpy)(CO)$_3$($\mathbf{H_2}$-L)]$^+$ with those of $\mathbf{Me_2}$-L and $\mathbf{H_2}$-L. Taken together, the data confirm that the decrease in emission intensity observed for [Re(bpy)(CO)$_3$($\mathbf{H_2}$-L)]$^+$ with increasing pH is caused by the deprotonation of the OH group in the *ortho*-position of the catecholamide unit. The ground state protonation constants and excited state inflection points obtained for [Re(bpy)(CO)$_3$($\mathbf{H_2}$-L)]$^+$/[Re(bpy)(CO)$_3$(H-L)] from the pH-profiles of the absorption and emission data, respectively, are lower than those obtained for $\mathbf{H_2}$-L/HL$^-$, which is consistent with the positive charge of the protonated sensor molecule and the electron withdrawing effect of the electron poor, rhenium-coordinated pyridine unit in [Re(bpy)(CO)$_3$($\mathbf{H_2}$-L)]$^+$.

As evident from Figures 5 and 9, the ligand is not emissive if fully protonated, but emits after deprotonation at 470 nm if excited into the catecholate-dominated absorption band at 360 nm. Although the excitation wavelength of the latter is very similar to the optimum excitation wavelength of the molybdate sensor (370 nm), no interference from ligand-based fluorescence is observed in the emission spectra of [Re(bpy)(CO)$_3$(H-L)]. The absence of the ligand fluorescence in the sensor may be due to the intramolecular heavy-atom effect of the Re leading to a shortening of the lifetime of the ligand-based excited states, but it could also be the result of photo-induced electron transfer (PeT) from the electron-rich catecholate-donor to the Re(bpy)-based acceptor (see below).

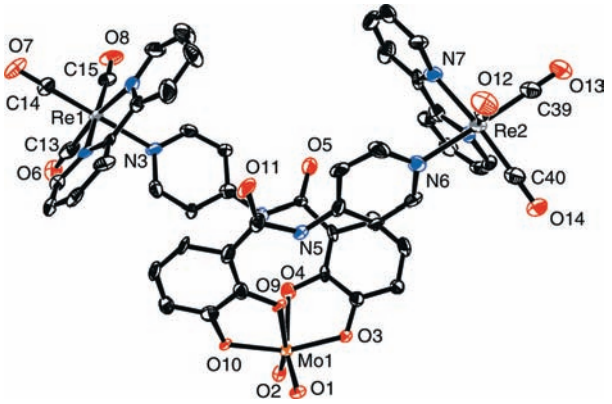

Figure 11. ORTEP plot of the molecular structure of $[MoO_2\{Re(bpy)(CO)_3(\mathbf{L})\}_2]$ (hydrogen atoms and lattice solvent molecules not shown).

The long-wavelength emission observed at 565 nm for $[Re(bpy)(CO)_3(\mathbf{H_2\text{-}L})]^+$ upon excitation at 370 nm in acidic solutions involves the metal center and is due to emission from the Re(dπ)→bpy ^{3}MLCT excited state. The absorption spectroscopic study showed that under alkaline conditions the MLCT absorption in the spectra of $[Re(bpy)(CO)_3(\mathbf{H\text{-}L})]$ overlaps with the catecholate-dominated intraligand-based transitions, which leads to an increase in absorbance at the excitation wavelength of 370 nm. The resulting competition contributes to the observed decrease of the emission intensity at 565 nm upon addition of base. In addition, intramolecular PeT from the deprotonated catecholate-donor to the Re(bpy)-acceptor may lead to the quenching of the emission from the Re^{II}-bpy* ^{3}MLCT state. Further evidence for PeT obtained from time-resolved IR and emission spectroscopy will be reported in a follow-up paper.

4. Reaction of $[Re(bpy)(CO)_3(\mathbf{H_2\text{-}L})]^+$ with Molybdate and Molecular Structure of $[MoO_2\{Re(bpy)(CO)_3(\mathbf{L})\}_2]$. The intensity of the emission from the Re^{II}-bpy* ^{3}MLCT excited state of $[Re(bpy)(CO)_3(\mathbf{H_2\text{-}L})]^+$ also decreases in the presence of molybdate, showing that the complex acts as a molybdate sensor. As previously reported,[23] the decrease in emission intensity upon titration of $[Re(bpy)(CO)_3(\mathbf{H_2\text{-}L})]^+$ with a solution of sodium molybdate is linear up to a break at a Mo/sensor ratio of 0.5, which is consistent with the formation of a 1:2 complex that contains a molybdenum center with two coordinated sensor molecules. The composition of the molybdenum-complex formed in solution was now confirmed by ESI-MS, and the structural features of the 1:2 complex in the solid state were identified by X-ray crystallography.

The ESI-MS investigation was carried out by reacting 2 equiv of $[Re(bpy)(CO)_3(\mathbf{H_2\text{-}L})]^+$ and 1 equiv of potassium molybdate in aqueous DMF (5% water). After equilibration, the only Re- and Mo-containing peaks observed correspond to the sodium or potassium adducts of the 1:2 complex $[MoO_2\{Re(bpy)(CO)_3(\mathbf{L})\}_2]$. The isotopic distribution patterns obtained for the two adducts match those calculated for the respective elemental compositions (Figure 10).

Reaction of 2 equiv of $[Re(bpy)(CO)_3(\mathbf{H_2\text{-}L})]^+$ with 1 equiv of sodium molybdate in aqueous acetonitrile (33% water) yielded a red solution from which deep red single crystals of $[MoO_2\{Re(bpy)(CO)_3(\mathbf{L})\}_2]$ suitable for X-ray crystallography could be obtained at pH 6. The molecular structure of the complex is shown in Figure 11; selected bond angles and distances are given in Table 3.

Table 3. Selected Bond Distances (Å) and Angles (deg) for $[MoO_2\{Re(bpy)(CO)_3(\mathbf{L})\}_2]\cdot CH_3CN\cdot 7(O)$

Bond Distances			
Mo(1)−O(2)	1.685(9)	N(1)−Re(1)	2.162(11)
Mo(1)−O(1)	1.720(9)	N(2)−Re(1)	2.163(11)
Mo(1)−O(10)	1.978(8)	N(3)−Re(1)	2.204(10)
Mo(1)−O(3)	1.980(8)	N(6)−Re(2)	2.203(10)
Mo(1)−O(4)	2.170(8)	N(7)−Re(2)	2.197(11)
Mo(1)−O(9)	2.172(7)	N(8)−Re(2)	2.151(10)
C(13)−O(6)	1.154(16)	C(38)−O(12)	1.194(17)
C(13)−Re(1)	1.901(16)	C(38)−Re(2)	1.873(18)
C(14)−O(7)	1.160(14)	C(39)−O(13)	1.111(15)
C(14)−Re(1)	1.894(13)	C(39)−Re(2)	1.939(15)
C(15)−O(8)	1.139(16)	C(40)−O(14)	1.162(15)
C(15)−Re(1)	1.925(16)	C(40)−Re(2)	1.918(15)
Bond Angles			
C(13)−Re(1)−C(15)	89.8(6)	C(40)−Re(2)−C(39)	89.3(6)
N(1)−Re(1)−N(2)	74.4(4)	N(8)−Re(2)−N(7)	74.6(4)
C(14)−Re(1)−N(3)	175.2(5)	C(39)−Re(2)−N(6)	176.3(5)
(1)-Mo(1)−O(2)	104.0(4)	O(3)−Mo(1)−O(4)	75.5(3)
O(9)−Mo(1)−O(10)	75.4(3)	O(3)−Mo(1)−O(10)	159.3(3)

The structural analysis revealed that two fully deprotonated sensor molecules are bound to a *cis*-dioxo-MoO_2 center via their catecholate-units in accord with the evidence from the ESI mass spectra and the emission titration. The resulting complex has approximate C_2 symmetry. Formally, $[MoO_2\{Re(bpy)(CO)_3(\mathbf{L})\}_2]$ is zwitterionic with the *cis*-dioxo-$MoO_2(cat)_2$-center bearing a 2− charge while each $Re(bpy)(CO)_3$(py)-center carries a positive charge. The crystal contained seven water molecules, two of which were modeled with 50% occupancy over two sites. The distorted octahedral geometry of the Mo-center is typical for MoO_2^{2+} core structures.[43] The strong π-donor character of the two terminal oxo ligands (O(1) and O(2)) leads not only to their *cis*-orientation but also to the binding of the weaker 2-benzoxy donors of the ligands (O(4) and O(9)) *trans* to them. This results in a lengthening of the Mo(1)−O(4) and Mo(1)−O(9) bonds in *trans*-position (2.170(8) and 2.172(7) Å, respectively), compared to the bonds *cis* to the oxo groups, Mo(1)−O(3) and Mo(1)−O(10) (1.980(8) and 1.978(8) Å, respectively). These bond lengths are comparable to those reported for other dioxomolybdenum(VI) complexes with catecholamide ligands.[31,44−47] The molybdenum−oxygen bond angles are also similar.

The two rhenium centers in $[MoO_2\{Re(bpy)(CO)_3(\mathbf{L})\}_2]$ show the characteristically distorted octahedral coordination geometry of bipyridine coordinated *fac*-$Re^I(CO)_3$ units, as previously observed for

(43) Stiefel, E. I. In *Comprehensive Coordination Chemistry*; Wilkinson, G., Ed.; Pergamon Press: Oxford, U.K., 1987; p 1380.
(44) Albrecht, M.; Franklin, S. J.; Raymond, K. N. *Inorg. Chem.* **1994**, *33*, 5785.
(45) Duhme, A.-K.; Dauter, Z.; Hider, R. C.; Pohl, S. *Inorg. Chem.* **1996**, *35*, 3059.
(46) Duhme, A.-K. *J. Chem. Soc., Dalton Trans.* **1997**, 773.
(47) Duhme, A.-K. *Z. Anorg. Allg. Chem.* **1998**, *624*, 1922.
(48) Martí, A. A.; Mezei, G.; Maldonado, L.; Paralitici, G.; Raptis, R. G.; Colón, J. L. *Eur. J. Inorg. Chem.* **2005**, 118.
(49) Lazarides, T.; Miller, T. A.; Jeffery, J. C.; Ronson, T. K.; Adams, H.; Ward, M. D. *Dalton Trans* **2005**, 528.

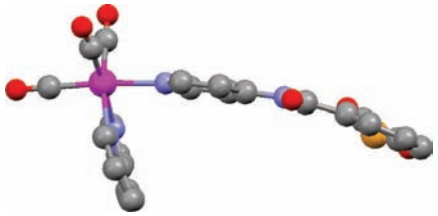

Figure 12. Ball and stick representation of a fragment of $[MoO_2\{Re(bpy)(CO)_3(\mathbf{L})\}_2]$ that illustrates the bending of one of the catechol ligands out of the pyridine plane (Re: magenta, Mo: orange, C: gray, N: blue, O: red).

$[Re(bpy)(CO)_3(\mathbf{Bn_2\text{-}L})]^+$.[23] The Re−C and Re−N distances are within the expected range.[48−51] The two ligands **L** in $[MoO_2\{Re(bpy)(CO)_3(\mathbf{L})\}_2]$ each contain an intramolecular hydrogen bond between the amide proton and the adjacent 2-benzoxy donor (distances N(4)···O(4) = 2.683(13) Å and N(5)···O(9) = 2.650(12) Å). The catechol and pyridine rings in the two ligands deviate significantly from an ideal coplanar orientation although the deviation is due to bending of the ligands rather than twisting (Figure 12). The structural parameters exclude a radical complex formulation as $[Mo(IV)O_2\{Re(bpy)(CO)_3(\mathbf{L}^{\cdot-})\}_2]$.

5. Conclusions. The pyridine-appended catecholamides **Me_2-L** and **H_2-L** were synthesized and characterized. The investigation of the photophysical properties of their accessible protonation states revealed important spectroscopic characteristics relevant to the signaling mechanism of the molybdate sensor $[Re(bpy)(CO)_3(\mathbf{H_2\text{-}L})]^+$. In acidic solution the molybdate sensor exhibits typical MLCT absorption and emission bands. After deprotonation of the catecholate-unit, ligand-based transitions overlap with Re(dπ)→bpy MLCT transitions. The quenching of both ligand-based fluorescence and emission from the Re(dπ)→bpy ^{3}MLCT state under alkaline conditions is consistent with a heavy atom effect and photoinduced electron transfer from the electron-rich catecholate to the Re(bpy)-based acceptor. In addition, **H_2-L** was found to be an interesting donor−acceptor system in its own right with three states of protonation and photophysical behavior suitable for pH sensing by absorption or emission. Finally, the formation of the dioxo-Mo(VI)Re_2 complex $[MoO_2\{Re(bpy)(CO)_3(\mathbf{L})\}_2]$ upon reaction of the sensor $[Re(bpy)(CO)_3(\mathbf{H_2\text{-}L})]^+$ with molybdate was ascertained in solution and in the solid state. The crystal structure determination revealed that two fully deprotonated sensor molecules are bound via their catecholate units to a *cis*-dioxo-MoO_2 center. Hydrogen bonds are formed between the amide proton and the 2-benzoxy donor of each ligand.

Acknowledgment. We thank the EU (Aquachem Marie Curie Research Training Network and COST D35- STSM-03115) and the K&A Wallenberg Foundation for financial support, Drs. J. Gun and O. Lev, The Hebrew University of Jerusalem, for preliminary mass spectrometry data and Ms. Juliet Morgan for experimental assistance.

Supporting Information Available: Figures S1 (^{1}H NMR spectra of $[H_3\text{-}L]^+$, $H_2\text{-}L$ and $H\text{-}L^-$), S2 (Absorption spectra of $[Re(bpy)(CO)_3(\mathbf{Bn_2\text{-}L})]^+$), S3 (Transient absorption spectra obtained for **H_3-L**$^+$ at pH 3.7), and X-ray crystallographic data for $[MoO_2\{Re(bpy)(CO)_3(L)\}_2]\cdot CH_3CN\cdot 7(O)$ in CIF format. This material is available free of charge via the Internet at http://pubs.acs.org.

(50) Yam, V. W.-W.; Chong, S. H.-F; Cheung, K.-K. *Organometallics* **2000**, *19*, 5092.
(51) Busby, M.; Gabrielsson, A.; Matousek, P.; Towrie, M.; Di Bilio, A. J.; Gray, H. B.; Vlček, A., Jr. *Inorg. Chem.* **2004**, *43*, 4994.